

Control Strategy Design of Active Magnetic Levitation Bearing for High-speed Flywheel Energy Storage Device

Pengwei Wang, Tianqi Gu, Binbin Sun, Rui Dang, Zhenwei Wang, Weichong Li, Tiezhu Zhang and Yang Wang

Abstract—With the advantages of high power density, high efficiency and long life, high-speed flywheel energy storage devices have been used in aerospace and transportation. Active magnetic levitation bearing is a key component that affects the performance of high-speed flywheel cells in terms of efficiency, stability and lifetime. The core specification of the active magnetic levitation bearing is the ability to control the flywheel rotor position based on external excitation to levitate it at the target position. Based on the principle of differential control, this paper designs the electromagnetic force control scheme in the vertical direction of the active magnetic bearing, and deduces the functional relationship between the upper and lower electromagnetic force and the position deviation. Then, based on Maxwell's electromagnetism, a simplified electromagnetic force model between the stator and rotor of the active magnetic levitation bearing is established, the control transfer function with current as input and displacement as output is derived, and the control characteristic equations are determined. Further, the PID control parameters are adjusted according to the Rouse criterion, and the ranges of the PID control parameters are derived and determined to meet the stability control requirements. Finally, the support characteristics and dynamic

response characteristics of the active magnetic levitation bearing are tested and analyzed. The results show that the designed control strategy can ensure that the active magnetic levitation bearing can levitate the flywheel rotor according to the operational requirements when subjected to external step and sinusoidal excitation. Under the step excitation, the rotor first reaches the target position in 0.009 s and enters the steady state in 0.057 s. Under the sinusoidal excitation, the overshoot is controlled within 0.5 % and the time lag is controlled within 0.1 ms.

Index Terms—high-speed flywheel battery, active magnetic levitation bearing, differential control, PID control

I. INTRODUCTION

High-speed flywheel energy storage device uses the increase and decrease of flywheel kinetic energy to achieve energy replenishment and output, which is different from chemical energy storage devices such as lithium batteries and NiMH batteries, and is a physical energy storage device [1-2]. Analyzed from the perspective of energy input and output methods, the common high-speed flywheel energy storage devices can be summarized as two types: electric storage type and mechanical type, mainly designed for power system power regulation, satellite attitude control, vehicle driving or braking, etc [3-4]. Among them, high energy storage and low self-consumption are the key parameters to measure the performance of high-speed flywheel devices, which need to be realized through the design and control of high-speed and high-efficiency flywheel rotor [5].

Due to the high rotor speed of the high-speed flywheel energy storage device, the conventional mechanical bearings will suffer from high friction loss and poor stability at high speed [6]. Active magnetic levitation bearings use the current magnetic effect to generate electromagnetic force, which can achieve stable levitation of the high-speed flywheel rotor in the target position and ensure the high-speed work of the flywheel rotor, and the rotor support parts have the characteristics of no contact, which can realize the efficient and stable operation of the high-speed flywheel rotor [7]. The design of active magnetic levitation bearing includes the basic structure, excitation method and control strategy. Among them, the basic structure and excitation method are the key to ensure that the active maglev meets the static levitation design index, and the control strategy design is the key to ensure the dynamic and stable operation of the active maglev bearing [8].

Currently, active maglev bearing control involves two parts: maglev bearing dynamics modeling and control

Manuscript received June 28, 2022; revised October 15, 2022.

This work was supported in part by the Innovation team project of "Qing-Chuang science and technology plan" of colleges and universities in Shandong Province 2021KJ083, the Major Innovation Projects in Shandong under Grant 2020CXGC010405 and 2020CXGC010406, the National Natural Science Foundation Project of China under Grant 51805301 and 52102465, the Postdoctoral Science Foundation of China and Shandong under Grant 2020M680091 and 202003042.

Pengwei Wang is a Professor of School of Transportation and Vehicle Engineering, Shandong University of Technology, Zibo, 255000 PR China. (e-mail: wpwk16@163.com).

Tianqi Gu is a graduate student of School of Transportation and Vehicle Engineering, Shandong University of Technology, Zibo, 255000 PR China. (e-mail: tianqi.gu@outlook.com).

Binbin Sun is a Professor of School of Transportation and Vehicle Engineering, Shandong University of Technology, Zibo, 255000 PR China. (corresponding author to provide phone: 86-13708941464; e-mail: sunbin_sdut@126.com).

Rui Dang is a graduate student of School of Transportation and Vehicle Engineering, Shandong University of Technology, Zibo, 255000 PR China. (e-mail: 18953820262@163.com).

Zhenwei Wang is a graduate student of School of Transportation and Vehicle Engineering, Shandong University of Technology, Zibo, 255000 PR China. (e-mail: zhenweiwang2022@163.com).

Weichong Li is a graduate student of School of Transportation and Vehicle Engineering, Shandong University of Technology, Zibo, 255000 PR China. (e-mail: 117616530216@163.com).

Tiezhu Zhang is a Professor of School of Transportation and Vehicle Engineering, Shandong University of Technology, Zibo, 255000 PR China. (e-mail: qdzhangtz@163.com).

Yang Wang is a graduate student of School of Transportation and Vehicle Engineering, Shandong University of Technology, Zibo, 255000 PR China. (e-mail: goodluck4wy@163.com).

strategy design. To achieve high precision and stable control of active maglev bearings, there are intelligent control methods such as constant vector control, LQR control, and neural network control [9-12]. Although such intelligent control methods can solve the nonlinear control problem of magnetic levitation bearings, they have the problem of limited real-time performance for engineering applications. To meet the requirements of engineering applications, this paper designs an active magnetic levitation bearing control strategy based on differential control and PID control, and analyzes and verifies its support characteristics and dynamic response characteristics.

II. ACTIVE MAGNETIC LEVITATION BEARING DIFFERENTIAL CONTROL SCHEME DESIGN

As shown in Fig. 1, the active magnetic levitation bearing designed in this research includes rotor, stator, coil winding, controller, position sensor, and power amplifier parts. The position sensor detects the rotor position in real time and transmits the signal to the controller. By calculating the deviation of the rotor position from the target position, the controller outputs the control signal according to the set control strategy. The control signal passes through the power amplifier and regulates the control current in the coil winding, thus changing the magnitude of electromagnetic force to achieve stable suspension control of the rotor at the target position. Since the designed active magnetic levitation bearing only needs to control the vertical direction displacement degrees of freedom, this paper uses a differential control scheme to achieve the levitation control of the magnetic levitation bearing in the vertical direction.

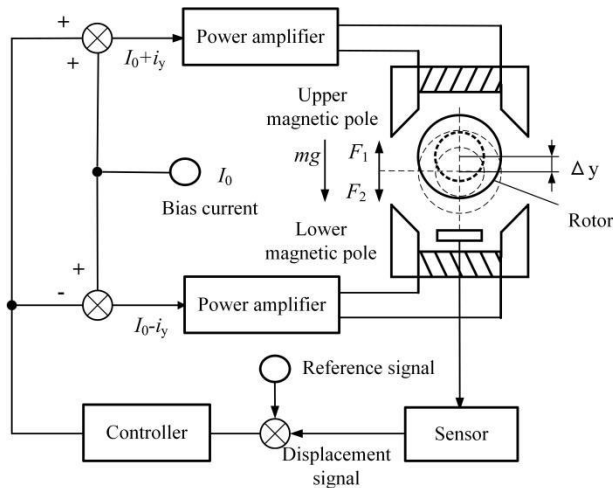


Fig. 2 Closed-loop differential control scheme for magnetic levitation bearings

As shown in Fig. 2, the designed differential control scheme is shown. In the vertical Y-direction, there are electromagnets consisting of a pair of poles on the top and bottom of the rotor, and the electromagnetic force in the Y-direction is generated to make the rotor upward and the electromagnetic force to make the rotor downward, respectively, and the two electromagnetic forces work together to control the rotor motion in this direction. When the spindle together with the magnetically levitated bearing

rotor is excited by external vibration, the rotor leaves the equilibrium position and produces a displacement offset Δy in the vertical direction, and the air gap values between the upper and lower poles of the stator and the rotor become $(y_0 + \Delta y)$ and $(y_0 - \Delta y)$, and the bias current in the coil winding is superimposed on the control current and becomes $(I_0 + i_y)$ and $(I_0 - i_y)$. The change in current causes the electromagnetic force generated by the corresponding solenoid to change, and the combined force changes to eventually return the rotor to the ideal equilibrium position.

According to the simplified mechanical model of magnetic levitation bearing, ignoring the effects of leakage and hysteresis, the electromagnetic force of the upper and lower pole electromagnets of the stator can be deduced. Among them, in the Y direction, the magnitude of the electromagnetic force generated by the upper electromagnet is as follows.

$$F_1 = \frac{\mu_0 A_0 N^2}{2} \frac{(I_0 + i_y)^2}{(y_0 + \Delta y)^2} \cos \alpha \quad (1)$$

In the Y direction, the magnitude of the electromagnetic force generated by the electromagnet below is as follows.

$$F_2 = \frac{\mu_0 A_0 N^2}{2} \frac{(I_0 - i_y)^2}{(y_0 - \Delta y)^2} \cos \alpha \quad (2)$$

Without considering external disturbing forces, the combined force on the rotor in the vertical Y direction is as follows.

$$F_y = F_1 - F_2 = \frac{\mu_0 A_0 N^2}{2} \left[\frac{(I_0 + i_y)^2}{(y_0 + \Delta y)^2} - \frac{(I_0 - i_y)^2}{(y_0 - \Delta y)^2} \right] \cos \alpha \quad (3)$$

Where, μ_0 is the vacuum permeability, N is the number of turns of the coil winding, A_0 is the stator pole area, α is half of the stator pole angle, Δy is the displacement offset, y_0 is the value of the air gap between the pole and the rotor, i_y is the control current, and I_0 is the fundamental bias current.

III. DERIVATION OF CONTROL CHARACTERISTIC EQUATIONS

Based on Maxwell's electromagnetism equation, the simplified electromagnetic force between the stator and rotor of the magnetic levitation bearing can be deduced as follows.

$$F = \frac{B_0^2 A_0}{\mu_0} \quad (4)$$

$$B_0 = \frac{\Phi_0}{A} = \frac{Ni}{\frac{l_s}{\mu_s} + \frac{l_r}{\mu_r} + \frac{2x}{\mu_0}} \quad (5)$$

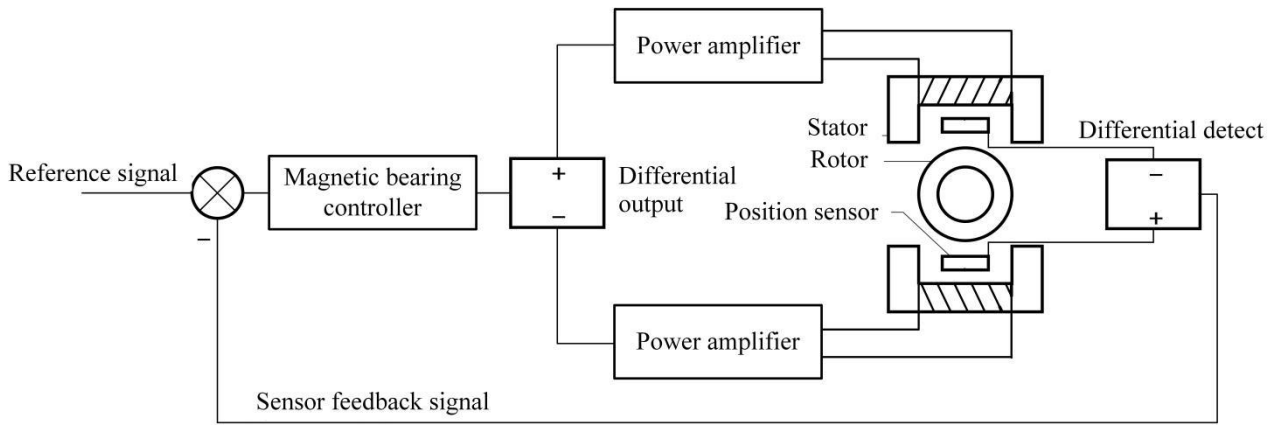


Fig. 1 Basic components and control principle of active magnetic bearings

Where, l_s is the magnetic circuit length of the magnetic levitation bearing stator, l_r is the magnetic circuit length of the magnetic levitation bearing rotor, x is the air gap value, i is the control current, μ_s is the magnetic permeability of the magnetic levitation bearing stator, μ_r is the magnetic permeability of the magnetic levitation bearing rotor, μ_0 vacuum permeability, and B_0 is the magnetic induction strength.

Considering the silicon steel material used for the stator and rotor of the maglev bearing, whose permeability is much higher than the vacuum permeability, $\mu_s \gg \mu_0$ and $\mu_r \gg \mu_0$, the following approximate derivation can be made.

$$\frac{l_s}{\mu_s} + \frac{l_r}{\mu_r} + \frac{2x}{\mu_0} \approx \frac{2x}{\mu_0} \quad (6)$$

At this point, the magnetic induction strength can be expressed as follows.

$$B_0 = \frac{\phi_0}{S_0} = \frac{NI}{\frac{l_s}{\mu_s} + \frac{l_r}{\mu_r} + \frac{2x}{\mu_0}} \approx \frac{NI}{\frac{2x}{\mu_0}} = \frac{\mu_0 NI}{2x} \quad (7)$$

In turn, the electromagnetic force between the stator and rotor of the simplified magnetic levitation bearing can be deduced.

$$F = \frac{\mu_0 A_0 N^2 I^2}{4x^2} \quad (8)$$

A Taylor expansion of the combined electromagnetic force on the rotor yields the force displacement function as follows.

$$F = k_i i + k_x x \quad (9)$$

In the above equation, $k_i = \frac{\mu_0 N^2 A I_0}{2x^2}$ is the current stiffness coefficient of the magnetic levitation bearing;

$k_x = \frac{\mu_0 N^2 A I_0^2}{2x^3}$ is the displacement stiffness coefficient of the magnetic levitation bearing.

Laplace transform is performed to obtain the transfer function with current as input $I(s)$ and displacement $X(s)$ as

output for a single degree of freedom in a magnetically levitated bearing as follows.

$$G(s) = \frac{X(s)}{I(s)} = \frac{k_i}{ms^2 - k_x} \quad (10)$$

The analysis shows that the characteristic equation of the controlled object has two poles and is located on the positive and negative real axes of the complex plane, which is an unstable second-order object and requires the addition of a closed-loop control link to eliminate the instability of the system. For this reason, the current control method based on PID closed-loop is used in this paper. Based on the basic theory of PID, the transfer function of the PID controller can then be deduced as follows.

$$G_c(s) = K_p + \frac{K_d s}{1 + T_d s} + \frac{K_i}{s} \quad (11)$$

The power amplifier plays the role of signal amplification, often using voltage-current type power amplifier. The control scheme adds a hysteresis link to simulate the transfer function of a voltage-current power amplifier.

$$G_a(s) = \frac{A_a}{1 + T_a s} \quad (12)$$

Where, A_a is the amplification coefficient of the power amplifier; T_a is the hysteresis coefficient of the power amplifier.

Displacement sensors mostly use eddy current displacement sensors, which convert the distance between the eddy current probe coil and the measured metal body into electrical parameters such as the equivalent inductance, equivalent impedance and quality factor of the coil, which are converted into voltage signals by the preamplifier in to achieve the measurement of displacement. In the feedback link of the magnetic levitation bearing system, the hysteresis link is added to simulate the transfer function of the eddy current displacement sensor.

$$G_s(s) = \frac{A_s}{1 + T_s s} \quad (13)$$

Where, A_s is the amplification coefficient of the

displacement sensor; T_s is the hysteresis coefficient of the displacement sensor.

The current signal comes from the control signal amplified by the controller, the power amplifier and the displacement transducer, which in turn allows the derivation of the transfer function.

$$I(s) = G_s(s)G_c(s)G_a(s)X(s) \quad (14)$$

In summary, the complete transfer function of the active magnetic levitation axis can be finally derived.

$$G(s) = \frac{\left(\frac{A_a}{1+T_a s}\right)\left(K_p + \frac{K_d s}{1+T_d s} + \frac{K_i}{s}\right)\left(\frac{k_{ix}}{ms^2 - k_{xx}}\right)}{1 + \left(K_p + \frac{K_d s}{1+T_d s} + \frac{K_i}{s}\right)\left(\frac{A_a}{1+T_a s}\right)\left(\frac{A_s}{1+T_s s}\right)\left(\frac{k_{ix}}{ms^2 - k_{xx}}\right)} \quad (15)$$

At this point, in order to pursue the system response speed, to ensure the selection of the controller proportional and differential coefficients, do not introduce the integral coefficient, the transfer function can be simplified as follows.

$$G(s) = \frac{\left(\frac{A_a}{1+T_a s}\right)\left(K_p + \frac{K_d s}{1+T_d s}\right)\left(\frac{k_{ix}}{ms^2 - k_{xx}}\right)}{1 + \left(K_p + \frac{K_d s}{1+T_d s}\right)\left(\frac{A_a}{1+T_a s}\right)\left(\frac{A_s}{1+T_s s}\right)\left(\frac{k_{ix}}{ms^2 - k_{xx}}\right)} \quad (16)$$

Further, the transfer function is simplified in order to facilitate the observation of the relationship between the control parameters and the displacement variables.

$$G(s) = \frac{a_4 s^4 + a_3 s^3 + a_2 s^2 + a_1 s^1}{b_5 s^5 + b_4 s^4 + b_3 s^3 + b_2 s^2 + b_1 s^1} \quad (17)$$

In the above equation, there are as follows.

$$\begin{cases} b_1 = A_a A_s K_p k_{ix} - k_{xx} \\ b_2 = k_{ix} (A_a A_s K_d + A_a A_s K_p T_d) - k_{xx} (T_a + T_d) \\ b_3 = m - k_{xx} T_d T_a \\ b_4 = m (T_a + T_d) \\ b_5 = m T_a T_d \end{cases} \quad (18)$$

IV. CONTROL PARAMETER ADJUSTMENT

According to the Rouse criterion, when the control system has stability, there exist positive real roots of its corresponding characteristic equation lying on the complex plane, i.e., all coefficients of the corresponding characteristic equation of the system are positive.

$$\begin{cases} A_a A_s K_p k_{ix} - k_{xx} > 0 \\ k_{ix} (A_a A_s K_d + A_a A_s K_p T_d) - k_{xx} (T_a + T_d) > 0 \\ m - k_{xx} T_d T_a > 0 \\ m (T_a + T_d) > 0 \\ m T_a T_d > 0 \end{cases} \quad (19)$$

Further, Rouse tables can be constructed.

s^5	b^5	b^3	b^1
s^4	b^4	b^2	b^0
s^3	A_1	A_2	0
s^2	B_1	B_2	0
s^1	C_1	0	0
s^0	D_1	0	0

Among them,

$$\begin{cases} A_1 = \frac{b_3 b_4 - b_2 b_5}{b_4} \\ A_2 = \frac{b_1 b_4 - b_0 b_5}{b_4} \\ B_1 = \frac{b_2 A_1 - b_4 A_2}{A_1} \\ B_2 = \frac{b_0 A_1}{A_1} = b_0 \\ C_1 = \frac{A_2 B_1 - A_1 B_2}{B_1} \\ D_1 = \frac{B_2 C_1}{C_1} = B_2 = b_0 \end{cases} \quad (20)$$

According to the system stability requirements, all parameters in the first column of the Rouse table have positive values, then

$$K_d + K_p T_d < \frac{m(T_a + T_d)}{A_a A_s T_d k_{ix}} \quad (21)$$

$$b_2 A_1 > b_4 A_2 \quad (22)$$

In summary, the range of values of the differential coefficient K_d can be obtained.

$$\begin{cases} K_d > \frac{s_2 - \sqrt{s_2^2 - 4s_1 s_3}}{2A_a A_s s_1 k_{ix}} + \frac{k_{xx}(T_a + T_d)}{A_a A_s k_{ix}} - K_p T_d \\ K_d < \frac{s_2 + \sqrt{s_2^2 - 4s_1 s_3}}{2A_a A_s s_1 k_{ix}} + \frac{k_{xx}(T_a + T_d)}{A_a A_s k_{ix}} - K_p T_d \end{cases} \quad (23)$$

Similarly, the range of values of the scale factor K_p can be obtained.

$$K_p \leq \frac{k_{ix}}{A_a A_s k_{ix}} + \frac{(m - k_{xx} T_d T_a)}{4m k_{xx} A_a A_s T_d T_a} \quad (24)$$

Finally, the range of controller parameters can be determined to meet the stability control requirements. After selecting the appropriate proportional parameters as well as the differential parameters in the range of values, a differential link is added to eliminate the hysteresis error according to the actual control effect.

$$\left\{ \begin{array}{l} 0 < T_a T_d < \frac{m}{k_x} \\ K_d + K_p T_d < \frac{m(T_a + T_d)}{A_a A_s T_a T_d k_i} \\ K_d > \frac{s_2 - \sqrt{s_2^2 - 4s_1 s_3}}{2A_a A_s s_1 k_{xx}} + \frac{k_x(T_a + T_d)}{A_a A_s k_i} - K_p T_d \\ K_d < \frac{s_2 + \sqrt{s_2^2 - 4s_1 s_3}}{2A_a A_s s_1 k_i} + \frac{k_x(T_a + T_d)}{A_a A_s k_i} - K_p T_d \\ K_p \leq \frac{k_i}{A_a A_s k_x} + \frac{(m - k_x T_a T_d)}{4mk_i A_a A_s T_d T_a} \\ K_p > \frac{k_x}{A_a A_s k_i} \end{array} \right. \quad (25)$$

V. PERFORMANCE TESTING AND ANALYSIS

A. Support characteristics analysis

The support characteristics of a magnetic levitation bearing are not only related to its own structure, but also to the control parameters of its controller. The support characteristics of the magnetic levitation bearing are analyzed based on the PID controller. Define the transfer function with the corresponding perturbation excitation as input and the rotor displacement as output for the generalized flexibility when the maglev bearing is disturbed as follows.

$$R(j\omega) = \frac{X(j\omega)}{F(j\omega)} = \frac{1}{k(j\omega)} = \frac{(k_i K_p - k_x) - jk_i \left(K_d \omega - \frac{K_i}{\omega} \right)}{(k_i K_p - k_x)^2 + k_i^2 \left(K_d \omega - \frac{K_i}{\omega} \right)^2} \quad (26)$$

Amplitude and frequency characteristics of the generalized flexibility.

$$|R(j\omega)| = \frac{1}{|k(j\omega)|} = \frac{1}{\sqrt{(k_i K_p - k_x)^2 + k_i^2 \left(K_d \omega - \frac{K_i}{\omega} \right)^2}} \quad (27)$$

Phase frequency characteristics of the generalized flexibility is as follows.

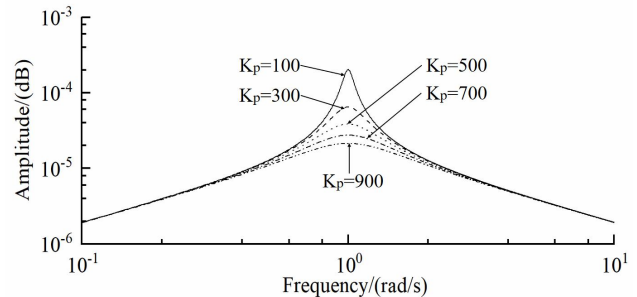
$$\varphi(\omega) = -\arctan \frac{k_i \left(K_d \omega^2 - K_i \right)}{\omega \left(k_i K_p - k_x \right)} \quad (28)$$

By calculating the variation of the generalized flexibility of the maglev bearing in the frequency domain, the influence of the PID controller control parameters on the support characteristics of the maglev bearing can be analyzed.

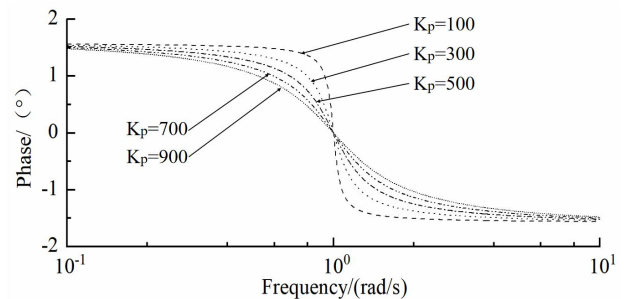
(1) Analysis of the influence of proportional parameters on the support characteristics

Keeping the integral and differential parameters of the controller unchanged, different scaling parameters were set to observe the effect on the support characteristics. Fig. 3 shows the frequency domain response curves of the magnetic levitation bearing PID controller under the unit step response function with different proportional

parameters, including the amplitude-frequency characteristic curve and the phase-frequency characteristic curve. For the maglev bearing PID controller, when the proportional parameter increases, the overall phase frequency curve tends to be flat, while the resonant frequency remains unchanged, the controller bandwidth is kept constant, and the phase lag at the resonant frequency is zero.



(a) Amplitude and frequency characteristics curve

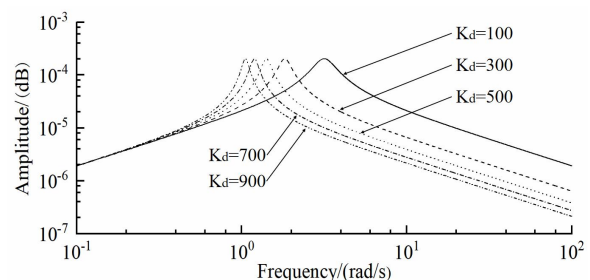


(b) Phase frequency characteristic curve

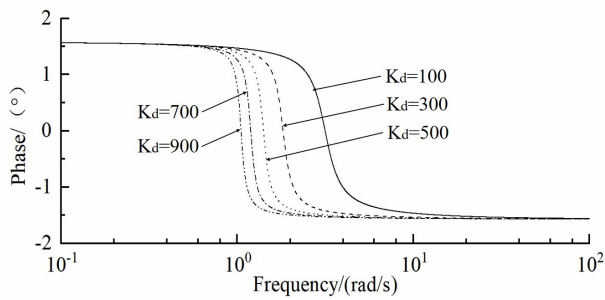
Fig. 3 Frequency domain characteristics of magnetic bearings under step response for changes in proportional parameters

(2) Analysis of the influence of differential parameters on the support characteristics

Keeping the integral and proportional parameters of the controller unchanged, different differential parameters were set to observe the effect on the support characteristics. Fig. 4 shows the frequency domain response curves of the magnetic levitation bearing PID controller under the unit step response function with different differential parameters, including the amplitude-frequency characteristic curve and the phase-frequency characteristic curve. For the magnetic levitation bearing PID controller, the effect of the differential parameter change is mainly in the high frequency band of the amplitude-frequency characteristic curve. When the differential parameter increases, the frequency domain response amplitude remains unchanged and the resonant frequency tends to be in the low frequency band, accordingly, the controller bandwidth becomes narrower and the response speed decreases.



(a) Amplitude and frequency characteristics curve

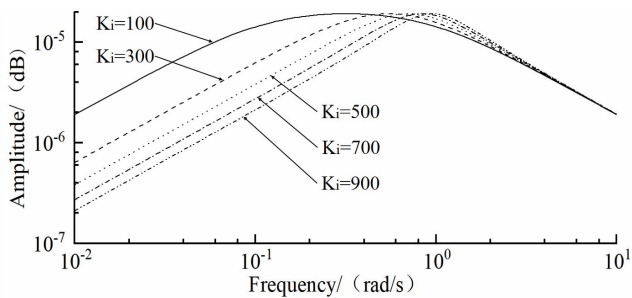


(b)Phase frequency characteristic curve

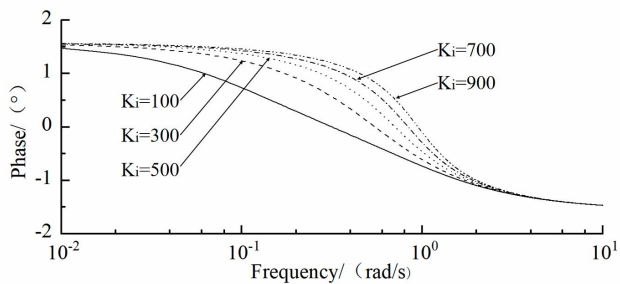
Fig. 4 Frequency domain characteristics of magnetically levitated bearings under step response for changes in differential parameters

(3) Analysis of the influence of integral parameters on the support characteristics

Keeping the proportional and differential parameters of the controller unchanged, different integral parameters were set to observe the effect on the support characteristics. Fig. 5 shows the frequency domain response curves of the magnetic levitation bearing PID controller under the unit step response function with different integration parameters, including the amplitude-frequency characteristic curve and the phase-frequency characteristic curve. For the magnetic levitation bearing PID controller, when the integration parameter increases, there is a significant decrease in the frequency domain response amplitude in the low frequency band, the transition time decreases, and the amplitude-frequency characteristic curve expands to the low frequency band. In the high frequency band, the variation of the integration parameter has almost no effect on the amplitude-frequency characteristic curve and the phase-frequency characteristic curve.



(a) Amplitude and frequency characteristics curve



(b)Phase frequency characteristic curve

Fig. 5 Frequency domain characteristics of magnetically levitated bearings in step response with varying integral parameters

B. Dynamic Response Characterization

The tested active maglev bearing prototype test system is

shown in Fig. 6. The test system mainly includes an air compression device, a high-pressure storage tank, a pressure regulating device, a magnetic levitation bearing and its controller. The compressed air is fed into the high pressure storage tank through the air compression device, and the compressed air is introduced into the annular air channel at the end of the magnetic levitation rotor through the pressure regulating device. The rotor speed is controlled by controlling the pressure and flow rate of the compressed air to simulate the high speed operation of the flywheel rotor.

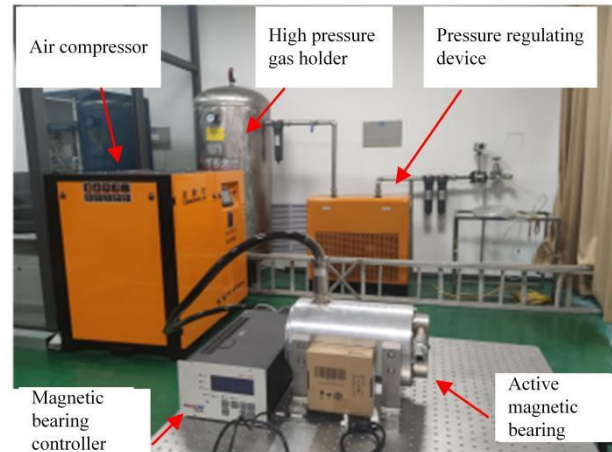


Fig. 6 Magnetic levitation bearing test prototype

The dynamic response of the bearing displacement and the control current variation characteristics of the maglev bearing under step and sinusoidal excitation are given in Fig. 7 and Fig. 8. The step signal and the sinusoidal periodic signal are applied to the controller as excitation to produce an offset of 0.1 mm according to the starting position of the magnetically levitated bearing rotor. From the step response results, it can be seen that the designed control strategy can realize the control of rotor undulation through the magnetic levitation bearing and can stabilize at 0.1 mm according to the required position signal, which achieves the requirement of stable levitation at the target position. Overall, the displacement overshoot is controlled within 0.14 mm, which satisfies the magnetic levitation bearing breath pitch requirement. The time for the rotor to reach the target position for the first time is 0.009 s, and the time to enter the steady state is 0.057 s, which meets the design requirements. From the sinusoidal response results, it can be seen that the displacement signal curve of the rotor output can effectively follow the control target requirements by applying a sinusoidal excitation of 12.5 Hz to the target. The overshoot is controlled within 0.5 % and the time lag is controlled within 0.1 ms.

VI. CONCLUSION

To ensure the efficient, safe and stable operation of the high-speed flywheel energy storage device, for the active magnetic levitation bearing, the differential control model of the flywheel rotor in the vertical direction is established in this paper. Then, combined with PID control theory, the control transfer function and characteristic equations of the current input and displacement output of the magnetic levitation bearing are derived, and the PID control parameters are rectified according to the Rouse criterion.

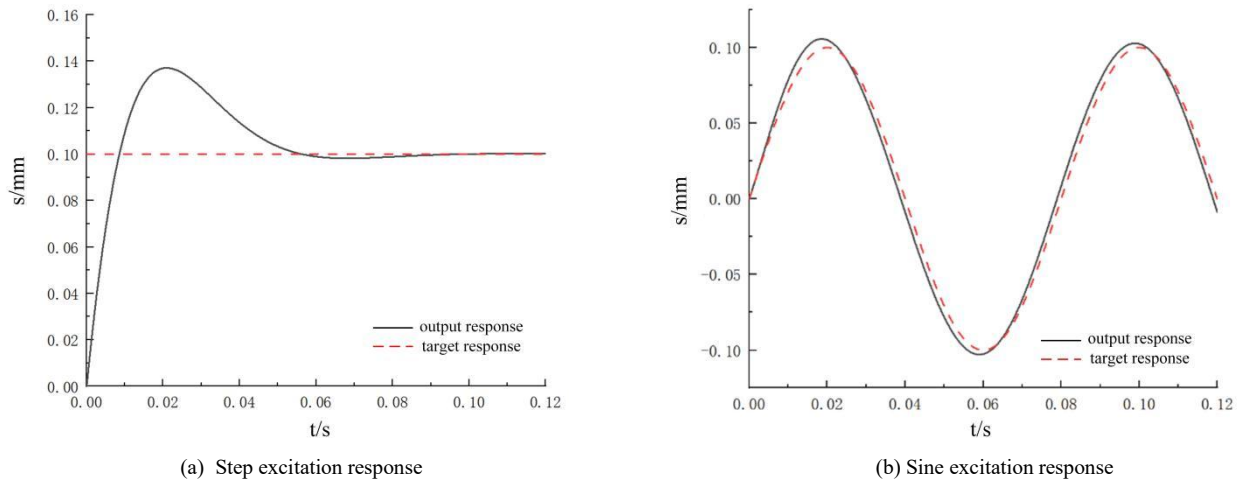


Fig. 7 Dynamic response characteristics of magnetically levitated bearings under step and sinusoidal excitation

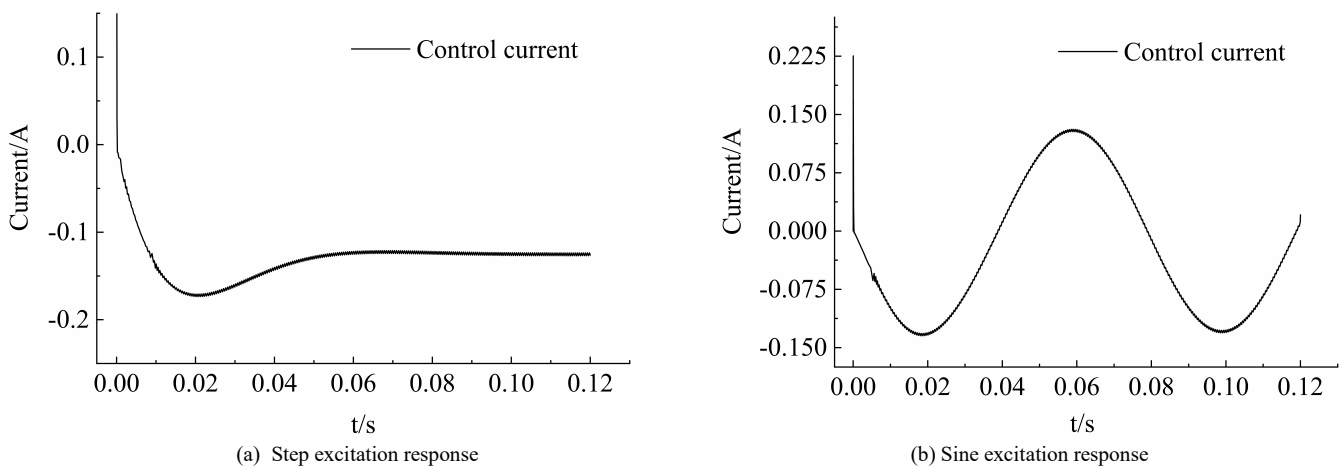


Fig. 8 Characteristics of magnetic levitation bearing control current variation under step and sinusoidal excitation

Finally, the relationship between the support characteristics of the maglev bearing and the PID control parameters is analyzed, and the dynamic response characteristics of the maglev shaft are tested. The following conclusions were obtained:

(1) When the scaling parameter increases, the phase frequency curve tends to flatten out, while the resonant frequency remains constant, the bandwidth remains the same, and the phase lag at the resonant frequency is zero. The effect of differential parameter variation is mainly manifested in the high frequency band of the amplitude-frequency characteristic curve. When the differential parameter increases, the frequency domain response amplitude remains the same, the resonant frequency tends to the low frequency band, the controller bandwidth becomes narrower, and the response speed decreases. When the integral parameter increases, the frequency response amplitude in the low frequency band decreases significantly, the transition time decreases, and the amplitude-frequency characteristic curve expands to the low frequency band. In the high frequency band, the variation of the integration parameter has almost no effect on the amplitude-frequency characteristic curve and the phase-frequency characteristic curve.

(2) Under the step excitation, the rotor first reaches the

target position in 0.009 s and enters the steady state in 0.057 s. Under the sinusoidal excitation, the overshoot is controlled within 0.5 % and the time lag is controlled within 0.1 ms. The designed control strategy can ensure that the active magnetic levitation bearing can achieve the levitation control of the flywheel rotor according to the operation requirements when it is affected by the external step and sinusoidal excitation.

REFERENCES

- [1] J. G. R. Hansen, D. U. O’Kain. An Assessment of Flywheel High Power Energy Storage Technology for Hybrid Vehicles[R]. Oak Ridge National Laboratory, 2012.
- [2] Mousavi G., Faraji F., Majazi A., et al. A comprehensive review of Flywheel Energy Storage System technology[J]. Renewable & Sustainable Energy Reviews, 2017, 67:477-490.
- [3] Olabi A. G., Wilberforce T., Abdelkareem M. A., et al. Critical Review of Flywheel Energy Storage System[J]. Energies, 2021, 14:2159.
- [4] Choudhury S.. Flywheel energy storage systems: A critical review on technologies, applications, and future prospects[J]. International Transactions on Electrical Energy Systems, 2021,31(9):1-16.
- [5] G. O. Cimuca, C. Saudemont, B. Robyns, et al. Control and Performance Evaluation of a Flywheel Energy-Storage System Associated to a Variable-Speed Wind Generator[J]. IEEE Transactions on Industrial Electronics, 2006, 53(4):1074-1085.
- [6] Zhang W., Wang J., Zhu P.. Design and analysis of a centripetal force type-magnetic bearing for a flywheel battery system[J]. Review of entific Instruments, 2018, 89(6):064708.

- [7] Yuan Y., Sun Y., Xiang Q.. Design and Analysis of a Magnetic Bearings with Three Degrees of Freedom[J]. Chinese Journal of Mechanical Engineering, 2019,32,(3):1-10.
- [8] Yu J., Zhou Y., Zuo H., et al. Stability Experiment of the High-Speed Active Magnetic Bearing-Flywheel System in the Rotating Frame[J]. Applied Computational Electromagnetics Society journal, 2019, 34(4):547-556.
- [9] Zhang L.L., Huang J. H.. Stability Analysis for a Flywheel Supported on Magnetic Bearings with Delayed Feedback Control[J]. Applied Computational Electromagnetics Society Journal, 2017, 32(8):642-649.
- [10] Ju J., Wang J., Wang Y., et al. Suspension force analysis of six-pole radial-axial magnetic bearing for energy storage flywheel[J]. International Journal of Modern Physics B, 2019, 34, 01n03:2040066
- [11] Basaran S., Sivrioglu S., Zergeroglu E.. Composite Adaptive Control of Single Gimbal Control Moment Gyroscope Supported by Active Magnetic Bearings[J]. Journal of Aerospace Engineering, 2017, 30(1):1-11.
- [12] Moises Jimenez-Martinez, "Artificial Neural Networks for Passive Safety Assessment," Engineering Letters, vol. 30, no. 1, pp289-297, 2022